Available online at www.sciencedirect.com
ScienceDirect
Applied Geochemistry 22 (2007) 1–16
Applied Geochemistry
www.elsevier.com/locate/apgeochem

Effective diffusion and microbiologic activity as constraints describing pyrite oxidation in abandoned lignite mines

Claus Kohfahl [a,*], Janek Greskowiak [b], Asaf Pekdeger [a]

[a] *Freie Universität Berlin, Institute of Geological Sciences, Malteserstr. 74-100, D-12249 Berlin, Germany*
[b] *Leibniz-Institut für Gewässerökologie und Binnenfischerei im Forschungsverbund Berlin e.V., Müggelseedamm 310, 12587 Berlin, Germany*

Received 5 March 2004; accepted 25 September 2006
Editorial handling by G. Ferris
Available online 20 November 2006

Abstract

This paper reports detailed O_2 measurements of pyrite bearing sediments in a column study and their interpretation based on a hydrogeochemical modelling approach. The research focuses on the quantitative effects of effective diffusion and microbiologic activity on pyrite weathering and acidification. A column experiment was set up and O_2 saturation and moisture contents were monitored over 100 days. The anoxic material used for the column experiment was taken from a sediment core of a mining waste dump in the southern periphery of the Lohsa storage system in the Lusatia region of Germany. The measured O_2 breakthrough curves were modelled using the simulator SAPY, a one-dimensional reactive transport code which considers the kinetics of chemical reactions and the delivery of O_2 into the sediment. The simulation yielded a strong dependence of pyrite oxidation on the moisture content which was quantified by an empirical equation. It was shown that the oxidation rate was catalysed by microbial activity exceeding the rate of diffusive O_2 delivery. In order to develop a management tool for predictive issues the results have already been applied to natural environments in another study using the adapted model.

1. Introduction

Brown coal surface mining pits are anthropogenically disturbed geological systems. Mineral reactions such as oxidation of primary Fe disulphides (pyrite, marcasite) release Fe, SO_4^{2-} and other minor but toxic elements to soil, surface water and groundwater. The main source of toxicity is the microbial mediated oxidation of Fe disulphides in the waste dump sediments due to penetration of O_2 and O_2-rich waters. Primary oxidation of the sediments begins during dewatering of the originally layered material prior to mining. Aeration is intensified during the mining process owing to excavation, mixing and dumping activities. After deposition, secondary pyrite oxidation continues in the aerated upper part of the spoils, possibly over a period of several decades. After decommissioning a mine, standard procedure is to allow the water table to rise and to

* Corresponding author.
E-mail address: kohfahl@zedat.fu-berlin.de (C. Kohfahl).

0883-2927/$ - see front matter © 2006 Elsevier Ltd. All rights reserved.
doi:10.1016/j.apgeochem.2006.09.003

convert the pit into a lake for recreational purposes. During flooding, which often extends over several years to decades, the acidity and other chemical contents in the groundwater are flushed into the newly formed lake and adjacent streams. Prediction of the future load mass of flushed acids and other chemicals requires detailed knowledge of the key processes controlling pyrite oxidation such as oxidation rates and delivery of O_2.

A number of column leach tests have been published in the literature. Two main experimental methods are commonly used in the laboratory to predict the generation of acid mine drainage. These are static tests which are carried out in a reaction chamber and column leach tests. Both tests provide information of mineral reactivity, acid generation rates and duration, metal dissolution, and other geochemical reactions including secondary mineral formation. A simple accelerated rock weathering method to predict acid generation kinetics using a static test has been published by Kargbo and He (2004). García et al. (2005) compared predictive weathering tests using columns of 1.5 m and static tests. Hecht and Kölling (2002) carried out column leach test with sediments containing 1.2 wt% pyrite monitoring the chemical composition of the leachate and the O_2 concentration in the column. Weber et al. (2004) performed column leach tests to investigate the geochemical effects of oxidation products and framboidal pyrite oxidation in acid mine drainage prediction techniques. These leach columns were run under the assumption that O_2 is freely available throughout the sample.

The oxidation rate of pyrite has been investigated in a number of studies. A rate law for Fe(II) oxidation under abiotic laboratory conditions was proposed by Stumm and Lee (1961). A review of earlier literature on abiotic chemical oxidation was presented by Lowson (1982). Nordstrom (1982) has reviewed the literature on both abiotic and biotic geochemical oxidation. The rate of Fe(II) oxidation is affected by numerous inorganic and biological parameters (Kirby and Elder Brady, 1998). The biogeochemical oxidation of Fe in natural systems may be mediated by a broad range of Fe-oxidising bacteria. It is well documented that *Thiobacillus ferrooxidans* catalyses Fe(II) oxidation such that at low pH, field rates can be 10^5–10^6 times faster than abiotic laboratory rates (Lacey and Lawson, 1970; Nordstrom, 1985). Optimal conditions for *Thiobacillus ferrooxidans* growth occur at pH values near 3 (Schnaitman et al., 1969). Several laboratory rates or rate laws which include *Thiobacillus ferrooxidans* terms have been proposed by Chavaire et al. (1993); Lacey and Lawson (1970); Nemati and Webb (1997); Nyavor et al. (1996); Okereke and Stevens (1991); Schnaitman et al. (1969). A modified Michaelis–Menten kinetics was used by Nemati and Webb (1997) to obtain a comprehensive Fe(II) oxidation rate law that includes temperature, Fe(II) and *Thiobacillus ferrooxidans* concentrations. This rate law was developed under O_2-saturated conditions, and pH was measured but not controlled, although the initial pH was 2.0. Another comprehensive rate law was presented by Pesic and Oliver (1989) which includes Fe(II), dissolved O_2, and *Thiobacillus ferrooxidans* concentrations, temperature, and pH.

Only few rates or rate laws have been published for Fe(II) oxidation at a field scale. For low pH conditions Nordstrom (1985) and Williamson and Rimstidt (1994) give a rate of approximately $5–10^{-7}$ mol L^{-1} s^{-1}, and Noike et al. (1983) give rates between 10^{-7} and 10^{-5} mol L^{-1} s^{-1}. Kirby and Elder Brady (1998) measured Fe(II) oxidation rates in untreated coal mine drainage and in wetland treatment systems using a continuously-stirred tank reactor; they found field rates ranging from less than 1×10^{-9} mol L^{-1} s^{-1} to 3.27×10^{-6} mol L^{-1} s^{-1}. No statistical correlation between pH, Fe(II), and dissolved O_2 and oxidation rates was found in this study, and no rate law was proposed. Hence there is no consensus on a rate law that applies in the field, nor is there consensus on which variables are most important in determining the field rate of Fe(II) oxidation in mine drainage.

The delivery of O_2 into the sediment is of major importance for pyrite weathering and the formation of acid mine drainage. Oxygen is delivered into the sediment by percolating oxygenated rainwater, and by diffusion and advection in the gas phase from the land surface boundary (Xu et al., 2000). Gaseous diffusion in the sediment occurs through the air porosity and is considered to be the most important process causing gaseous interchange between sediment and atmosphere (Troeh et al., 1982).

A number of models have been developed to study geochemical processes at mine sites. Some of these models consider equilibrium reactions and additional kinetic processes without considering diffusive O_2 delivery. Foos (1997) developed a geochemical model including reactive and conservative transport, equilibrium reactions, kinetic

reactions and adsorption. The geochemical model of Strömberg and Banwart (1994) includes kinetics of sulphide and primary silicate mineral weathering, heterogeneous equilibrium with secondary mineral phases and speciation equilibrium. Further models consider also the delivery of O_2into the sediment in combination with simplified kinetic approaches (Davis et al., 1986; Davis and Ritchie, 1986, 1987; Hecht et al., 2003; Schwan et al., 1988). One example is MINTOX (Wunderly et al., 1996) which combines the O_2 diffusion and sulphide oxidation model PYROX (Wunderly et al., 1996) with the geochemical equilibrium, reactive transport model MINTRAN (Walter et al., 1994a,b). The program PYROX also includes O_2 diffusion and transport reactions and is based on the shrinking core model developed by Davis and Ritchie (1986). MIN3P (Mayer, 2002) includes advective–dispersive transport in the water phase and diffusive gas transport coupled with geochemical reactions and a Monod formulation for microbial mediated reactions (Cornish Bowden, 2004). The program SAPY (Prein and Mull, 1998) which was applied in this research couples transport of the reactants by diffusion and advection in water and air with chemical reactions of pyrite weathering including pH dependent biological catalysis.

Owing to the great diversity of transport and chemical reaction phenomena, no universally accepted methodology for modelling such processes has emerged, or is likely to emerge. Instead, simulation methodology must be carefully chosen and tailored to the specific physical and chemical properties of the system being investigated, and to the objectives of the modelling study. These differ in their emphasis on accuracy and comprehensiveness of flow and transport modelling on the one hand, and chemical interactions between rocks and fluids on the other hand (Xu et al., 2000).

The present study was part of a larger investigation program, which aimed at predicting SO_4^{2-} charges released from the unsaturated zone of the waste dumps into the groundwater and the surrounding lakes for the next decades in the Lusatia region of Germany. This paper reports a column test, which was carried out in order to study the impact of O_2 delivery in the gas phase and microbial mediated oxidation rates on pyrite weathering. In contrast to column leach tests that have been published so far, this column study was carried out without irrigation to exclude O_2 delivery by percolating recharge water. To achieve a quantitative understanding of the relevant biogeochemical transport processes and to provide a quantitative modelling framework for up-scaling purposes, the one-dimensional multi-phase reactive transport code SAPY was applied. This tool was selected for the simulations because the SAPY code, in contrast to many other existing simulators, considers the pH dependent microbial mediated kinetics of pyrite oxidation. Furthermore Prein and Mull (1998) developed and verified the model based on field studies and laboratory experiments related to the Lusatian mining district. The program was tested and further modified on the basis of the laboratory data presented here.

2. Study area

The study area is the Lohsa lignite mine near Hoyerswerda in Germany (Fig. 1). This mine was exploited from 1970 to 1990, when its groundwater level was lowered artificially to a maximum depth of 50 m below subsurface. The pumped water was discharged into the Spree River during that period. Pumping of groundwater stopped after the mine was decommissioned, so the water level of the Spree River has declined since 1990, causing water quality problems for the drinking water supply in the downstream areas. The former lignite mine was to be flooded, mainly with surface water, by 2005 and afterwards used as a reservoir basin for equilibrating the Spree River water table. The waste dump material originates predominantly from Quaternary overburden of the second Lusatian coal seam which was exploited until 1990. The waste dump material is built up of fine grained sand and silt with small amounts of resedimented lignite fragments of Tertiary age. These coal splitters lead to comparatively low pyrite contents which are now subjected to weathering processes in the unsaturated zone of the surrounding 40 m-high waste dumps. This will lead to a continuous release of acidity and SO_4^{2-} into the groundwater, into the forming lake and into the Spree River.

Since the bank filtrate of the Spree is used for drinking water in urban areas downstream of Lohsa, the long-term release of SO_4^{2-} is of special interest. Owing to its conservative behaviour in this hydrogeochemical environment it may constitute a severe problem for the future drinking water supply.

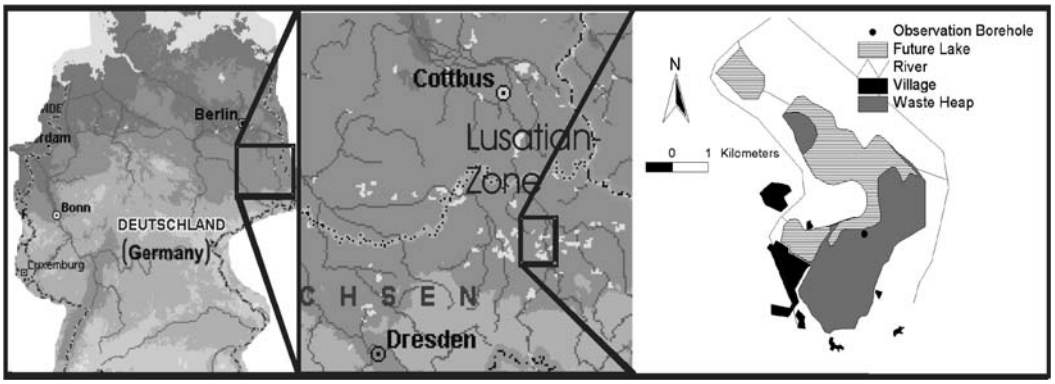

Fig. 1. Study area Lohsa. The sediment material for the column experiment was taken from a core drilled a few metres from the observation borehole, which was located approximately at a distance of 100 m from the lakeside at the time of sampling.

3. Methods

3.1. Sediments

The material used for the column experiments was taken from a core of a waste dump in the southern periphery of the former open-pit mine Lohsa II (Fig. 1). The anoxic material was taken from the water saturated zone at a depth of 23–25 m below surface and conserved under anoxic water saturated conditions in an airtight plastic liner. The material consisted of fine sands and lignite fragments.

Sulphide was extracted as acid volatile sulphide (AVS) using HCl and as pyrite using a Cr(III)Cl solution as extraction agent. The extraction with Cr(III)Cl includes pyrite-bound S as well as AVS phases. In contrast to conventional methods, the H_2S degassing in the acid environment was not blown out but transported into the Zn-acetate trap by passive diffusion over 48 h (Hsieh and Yang, 1989). Organic and inorganic C was determined with a C-N-S Analyzer (Leco). CEC was determined using the $BaCl_2$-method (Hendershot and Duquette, 1986). The mineralogical composition of a sediment sample of the upper part of the column was analysed by X-ray diffractometry after the column experiment. No detailed analysis of the column-sediment after the experiment was performed because the column study represents the first (drained) period of a long-term column test with subsequent flooding. Information about the grain size and surface area of pyrite in these sediments was obtained from Berger (2000).

3.2. Column experiment

The entire experiment was conducted to investigate the influence of water table oscillations on pyrite weathering by laboratory studies and reactive transport modelling. Hence, the column was drained in the first period of 100 days to allow pyrite weathering and acidification. Afterwards the column was flooded from bottom to top to study the hydrogeochemical evolution of the rising water table (Kohfahl and Pekdeger, 2006). This paper reports the results of the drainage period.

A plexiglass column (200 cm length, 10 cm i.d.) was prepared along the profile with 10 suction cups, 10 TDR-probes for measuring moisture content, and 20 fibre optic oxygen probes (Fig. 2). The technique for constructing the oxygen probes was developed by Hecht and Kölling (2001). To allow discharge and control of water level a lower outlet was prepared below the column. The water level was controlled by a transparent tube connected with the lower outlet. A 3 cm thick filter-layer of inert quartz sand was placed at the bottom of the column to distribute flow and to prevent obstruction by smaller particles. Immediately before packing the water saturated sediment was homogenised manually in a barrel for 1. To minimise contact with atmospheric O_2 1 L of anoxic distilled water was added during homogenisation. Afterwards the column was packed with the homogenised and water saturated sediment. In order to minimise advection, pore water extractions were carried out before draining the column. The samples were taken in the saturated zone at 110 and 120 cm depth using suction cups. Major cation analysis of pore water

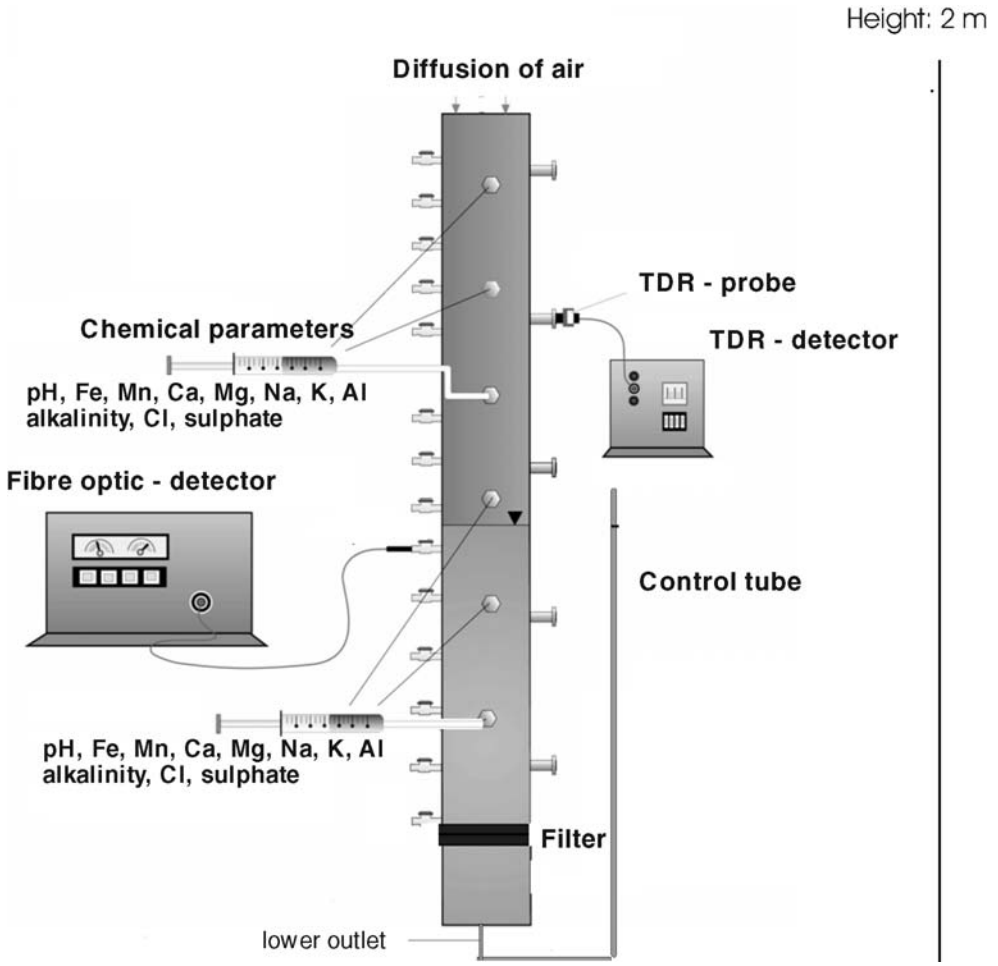

Fig. 2. Design of the column experiment. At the beginning of the experiment the water saturated column was discharged until a water level of 50 cm height was reached in the column. Chemical parameters were analysed only at a depth of 110 and 120 cm under saturated conditions before the column was drained.

was carried out on filtered acidified samples using ICP-AES (Perkin-Elmer AAS 5000), while major anions were determined using ion chromatography (Dionex DX-100). Iron was analyzed as total Fe.

After taking the samples, 3.3 L of water were discharged from the lower outlet until a hydraulic head of 50 cm height measured from the bottom of the column was reached. Oxygen saturation and moisture content were measured at different depths of the unsaturated zone in the column over a 100-day period. Moisture contents in the column were measured by time domain reflectometer (TDR probes; EASYTEST Fp/m) and O_2 of soil air and pore water was measured by an optical method using the optical fluorescence-method provided by PRESENS (MICROX 1). To restrict the O_2 delivery to the gas phase, the experiment was performed without irrigation of the column.

3.3. Numerical modelling

3.3.1. General aspects

Since no detailed English documentation about the applied software SAPY (Prein and Mull, 1998) has been published so far, a short description of the main aspects is given in the following. SAPY is a one-dimensional reactive transport model, that has been developed especially for the simulation of pyrite weathering. The numerical algorithm couples transport of the reactants by diffusion and advection in water and air with chemical reactions of pyrite weathering including biological catalysis.

The different phases of each cell are taken into account as follows:

- The gas phase by calculating the convective transport of air and the diffusive transport of O_2 and N_2.
- The water phase by calculating diffusive and convective transport of dissolved O_2 and reaction products (SO_4^{2-}, Fe^{2+} and H^+).
- The solid phase by calculating kinetically controlled mass transfer due to pyrite weathering.

Diffusive and convective transport of O_2 and weathering products is calculated by the method of finite differences. Since the column was not irrigated during the experiment, no transport of water and solutes had to be considered in the simulations.

Distribution of O_2 between water and atmosphere is calculated according to Henry's law. Production and consumption of O_2, Fe^{2+}, Fe^{3+}, SO_4^{2-}, FeS_2 and H^+ due to pyrite weathering are calculated according to Singer and Stumm (1970) based on the available amount of O_2 in water.

3.3.2. Diffusive transport in the gas phase

According to Fick's first law the diffusive flux of one gas into a reference gas can be calculated according to Crank (1956):

$$F = -D\frac{\partial C}{\partial x} \tag{1}$$

where F is flux ($M\ t^{-1}\ L^{-2}$), D represents the molecular diffusion coefficient in gas ($L^2\ t^{-1}$), ∂x is the straight line distance between the concentrations of two defined locations (L), and C is concentration in units of e.g. ($M\ L^{-3}$).

The molecular diffusion coefficient is corrected for temperature and pressure, moisture content and tortuosity. The influence of pressure and temperature is calculated according to a standard approach (Landolt-Börnstein, 1969).

$$D' = \left(D\frac{T}{273.16\,K}\right)^{1.82} \times \left(\frac{1013\,\mathrm{hPa}}{p}\right) \tag{2}$$

where D' means diffusion coefficient corrected for temperature and pressure (m^2/s), D is molecular diffusion coefficient in gas (m^2/s) at standard conditions, T is temperature in Kelvin and p is pressure in hecto Pascal (hPa).

Porous media form obstructions for the gaseous flow leading to actual path lengths longer than the straight line distance ∂x considered in Eq. (1). This is taken into account by the tortuosity which is defined as the ratio of the actual path length over the straight line distance. According to Currie (1970) the molecular diffusion coefficient has to be corrected as follows.

$$D'' = D'\frac{n_a}{\tau^2} \tag{3}$$

where D'' means effective diffusion coefficient ($L^2\ t^{-1}$), n_a is airfilled porosity (–), and τ represents tortuosity (–).

The tortuosity depends on the grain size distribution, the geometrical shapes of the particles and the moisture content. Albertsen (1977) carried out a number of diffusion experiments and derived empiric dependencies of tortuosity on water filled porosity for different types of sediments. According to his studies the water filled porosity constitutes the most sensitive parameter with much higher influence than grain size distribution and geometrical shapes of particles. In SAPY the calculation of tortuosity is based on an empiric formula derived by Albertsen (1977) for coarse grained sands as follows (Fig. 3):

$$\text{For } n_a/n > 0.2: \frac{1}{\tau^2} = 10^{\left(\left(\frac{n_a}{n}-1.126\right)/0.485\right)} \tag{4}$$

$$\text{For } n_a/n < 0.2: \frac{1}{\tau^2} = 10^{-4} \tag{5}$$

where n means total porosity (–).

3.3.3. Advective transport of gas

Driving forces for gas advection are temperature driven advection (Pantelis and Ritchie, 1991), changes in atmospheric pressure (Eberling et al., 1998) and volume changes of gas due to geochemi-

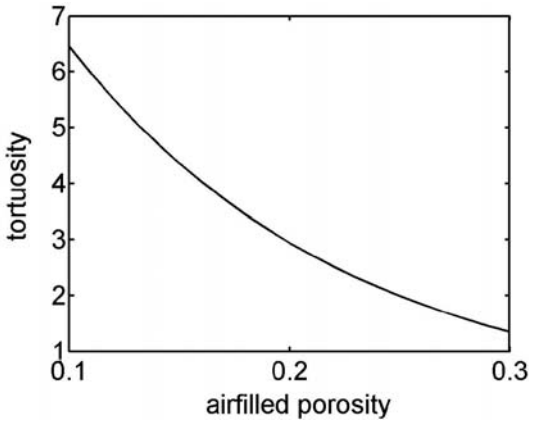

Fig. 3. Dependence of tortuosity on waterfilled porosity implemented in the original SAPY source code.

cal reactions. In this column study conducted under laboratory conditions negative pressures induced by the consumption of O_2 due to pyrite weathering are the main factors leading to advective gas transport.

Darcy's law, which was developed for water flow in saturated media, can also be applied to single phase gas flow. In SAPY the advective gas velocity was implemented by the authors according to Darcy's law after Scanlon et al. (2002)

$$J_g = -k_r \times \frac{k_g}{\mu_g} \times \frac{dp}{dz} \quad (6)$$

where J_g is the volumetric flux density of gas ($L^3\ L^{-2}\ t^{-1}$), k_g is the permeability (L^2), k_r is the relative gas permeability (–), p is pressure ($M\ L^{-1}\ t^{-2}$), z is elevation (L) and μ_g = gas viscosity ($M\ L^{-1}\ t^{-1}$).

The relative permeability is a function of the water saturation and is defined as the permeability of the unsaturated medium at a particular water saturation divided by the permeability at 0% water saturation. k_r was calculated after Falta et al. (1989)

$$k_r = (1 - S_l)^3 \quad (7)$$

where S_l stands for water saturation.

Test simulations with SAPY yielded an amount of advective transport in the gas phase of less than 5% which concurs with observations of other studies (Eberling and Nicholson, 1996; Simunek and Suarez, 1993).

3.3.4. Pyrite oxidation

According to Singer and Stumm (1970) the limiting step of the overall oxidation of pyrite is the oxidation of Fe^{2+}. The oxidation rate of Fe^{2+} is independent of pH for low pH values while in the higher pH range the dependence on $[OH^-]$ is of second-order.

The approximation of the oxidation rate defined by Singer and Stumm (1970) is realised in SAPY as follows (Fig. 4):

$$\frac{d[Fe^{2+}]}{dt} = k \times km \times k_T \times pO_2 \times [Fe^{2+}] \times \left(1 + \frac{[Fe^{2+}]}{K_i}\right)^{-1} \quad (8)$$

where [ ] indicates aqueous concentration ($M\ L^{-3}$), k is the abiotic reaction constant ($M^{-1}\ L^1\ t^1$), km is the microbial acceleration factor (–), k_T is the correction factor for temperature (–), K_i, is the inhibition factor ($M\ L^{-3}$), pO_2 is partial pressure of O_2 ($M\ L^{-1}\ t^{-2}$), t is time.

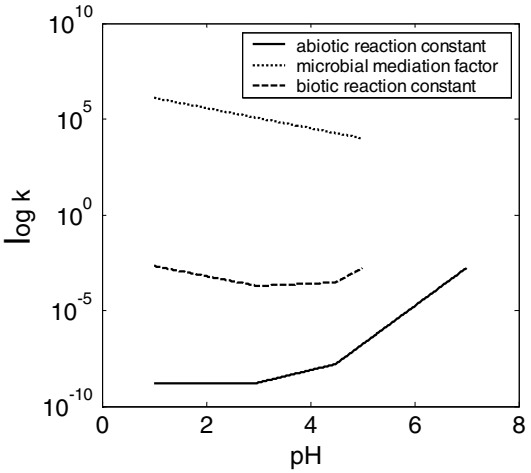

Fig. 4. Reaction constant for abiotic and microbial mediated oxidation of Fe(II) as a function of pH implemented in SAPY. k (hecto Pascal seconds)$^{-1}$ represents the abiotic/biotic reaction constant. The microbial acceleration factor km is dimensionless.

The dependence of the abiotic reaction constant k on pH is approximated in SAPY as follows:

pH < 3.0:

$$k = 1.67 \times 10^{-9} \quad (9)$$

3.0 < pH < 4.5:

$$k = \frac{10^{(0.65\,pH\,-8.94)}}{60} \quad (10)$$

pH > 4.5

$$k = \frac{10^{(2\,pH\,-15)}}{60} \quad (11)$$

Fig. 4 indicates that rates remain low for purely inorganic systems. However, bacteria such as *Thiobacillus ferrooxidans* are able to increase the Fe^{2+} oxidation rate by up to 5 orders of magnitude (Nordstrom, 1982). To account for the microbial acceleration the parameter k is multiplied by the dimensionless biological acceleration factor km. The calculation of km is a result of fitting experimental data of Kölling (1990) by Prein (1993). These experimental data describe the pore water chemistry of column studies carried out with lignite sediments of different sites in the Lusatian mining district. The dependency of km on pH takes into account the optimal milieu conditions for microbiologic activities in these sediments and is formulated in SAPY as follows (Fig. 4):

$$\text{For pH} \leqslant 5: \quad km = 10^{(-0.5264 \times \text{pH} + 6.632)} \tag{12}$$

$$\text{For pH} > 5: \quad km = 1 \tag{13}$$

These equations are in agreement with Lacey and Lawson (1970) and Nordstrom (1985) who detected that biologic activity starts with a pH lower than 5 and can be 10^5–10^6 times faster than abiotic laboratory rates at low pH.

Karavaiko et al. (1982) analysed the effect of Fe^{3+} on the oxidation rate for different temperatures and found that high concentrations of Fe^{3+} inhibit the reaction rate. They assume that Fe^{3+} is acting as a competitive oxidant for the microbial oxidation of Fe^{2+}. Curutchet (1992) supported these results. After Karavaiko et al. (1982) the inhibition factor for temperatures above 10 °C is calculated according to

$$K_i = (-0.82 \times T + 25.25) \times 1000 \tag{14}$$

For the temperature of 20 °C in the experiment the resulting inhibition factor of 8850 has only a minor influence on the calculated oxidation rate.

The biological acceleration is due not only to the metabolism of the individual microbiological species but also to the reproduction rate which is mainly dependent on temperature. This is taken into account by the parameter k_T and is calculated according to Ahonen and Tuovinen (1989).

$$k_T = 0.0047 \times (T - 6)^2 + 0.12 \tag{15}$$

where k_T is the dimensionless acceleration factor for temperature, T is temperature.

As the experiment was conducted with temperatures around 20 °C, the k_T-value is near 1 and only of minor importance for the simulations.

3.3.5. Discretisation, boundary conditions and initial conditions

The parameters defined for all cells in the simulations are compiled in Table 2. The one-dimensional model was subdivided in 20 cells of 0.1 m length. A constant atmospheric pressure was defined for the upper boundary; a no-flow boundary for gas flow was defined for the lower boundary. The initial geochemical parameters were derived from the analysis of sediments and water samples of the column experiment and were defined as start values for the simulation. According to the pore water composition before draining the column given in Table 3

Table 2
Discretisation, boundary conditions and input parameters defined for all cells

Number of cells	19
Vertical grid distance, m	0.1 m
Time step, sec	1
Upper boundary	Constant pressure
Lower boundary	No-flow boundary
Initial pyrite content (wt%)	0.04
Initial oxygen content (%)	0
Initial pH in all cells	5
Recharge (mm/a)	0
Total porosity, %	30
Buffering capacity	0
ρ_g (gas density) for 20 °C	1.2 kg m^{-3}
μ_g (gas viscosity) for 20 °C	1.8 10^{-5} Pa s
ρ_w (water density) for 20 °C	998 kg m^{-3}
μ_w (water viscosity) for 20 °C	1.0×10^{-3} Pa s
D (molecular diffusion coefficient at standard conditions)	9.61×10^{-6} m^2 s^{-1}
k_g (permeability)	10^{-14} m^2

Table 1
Chemical sediment parameters of the material used in the column study

Parameter	Unit		Analytical method
H^+	meq/100 g sediment	0.015	Batch experiment with H_2O
Na	meq/100 g sediment	0.14	CEC (diluted with $BaCl_2$)
K	meq/100 g sediment	0.21	CEC (diluted with $BaCl_2$)
Mg	meq/100 g sediment	0.22	CEC (diluted with $BaCl_2$)
Fe	meq/100 g sediment	0.02	CEC (diluted with $BaCl_2$)
Mn	meq/100 g sediment	0.02	CEC (diluted with $BaCl_2$)
Al	meq/100 g sediment	0.33	CEC (diluted with $BaCl_2$)
Ca	meq/100 g sediment	0.86	CEC (diluted with $BaCl_2$)
Organic C	wt%	0.50	Leco
Inorganic C	wt%	0.10	Leco
Pyrite content	wt%	0.04	Iodometrically
Monosulphidic S	wt%	0.0001	Iodometrically

H^+ is the concentration of protons which has been diluted by H_2O. CEC stands for cation exchange capacity.

Table 3
Analysed initial solution of the column (conc. are given in mmol/L)

pH	Temperature (°C)	Na	K	Ca	Mg	Fe	Mn	Cl	S(6)	Alkalinity	Al	E_h (mV)
5.0	20	0.96	0.18	6.24	2.02	2.15	0.09	1.35	9.13	0.3	not detected	123

an initial pH of 5 and a buffer capacity of 0 were defined. According to Landolt-Börnstein (1969) the molecular diffusion coefficient of O_2 in air for standard conditions (1 atm. and 25 ° C) was set to 9.1×10^{-6} m^2 s^{-1}. The gas permeability was set to 10^{-14} m^2 which is representative for very fine sands and mixtures of sand, silt and clay (Scanlon et al., 2002). The moisture contents stayed more or less constant during the experiment and ranged between 2 vol% in the upper TDR-probes and 10 vol% in the lower probes of the unsaturated zone (Fig. 5). The initial parameter distribution for all cells is given in Table 4.

3.3.6. Calibration

The value of tortuosity is difficult to calculate, because it depends strongly on pore size distribution, pore geometry and water content and shows great variations in natural sediments. Furthermore there are numerous approaches in the literature describing the influence of water saturation on tortuosities for different sediments (Albertsen, 1977; Marshall, 1959; Millington, 1960; Penman, 1940; Troeh et al., 1982). Hence the tortuosity is a site specific parameter and was used as a fitting parameter. The simulated breakthrough curves of O_2 were fitted to the measured results by changing the dependence of tortuosity on waterfilled porosities leading to different effective diffusion coefficients.

Table 4
Initial conditions of all individual cells

Depth (m)	Airfilled porosity	Water filled porosity
0.05	0.28	0.02
0.15	0.27	0.03
0.25	0.27	0.03
0.35	0.26	0.04
0.45	0.26	0.04
0.55	0.25	0.05
0.65	0.24	0.06
0.75	0.23	0.07
0.85	0.23	0.07
0.95	0.22	0.08
1.05	0.22	0.08
1.15	0.21	0.09
1.25	0.20	0.10
1.35	0.18	0.12
1.45	0.13	0.17
1.55	0.13	0.17
1.65	0.001	0.299
1.75	0.001	0.299
1.85	0.001	0.299
1.95	0.001	0.299

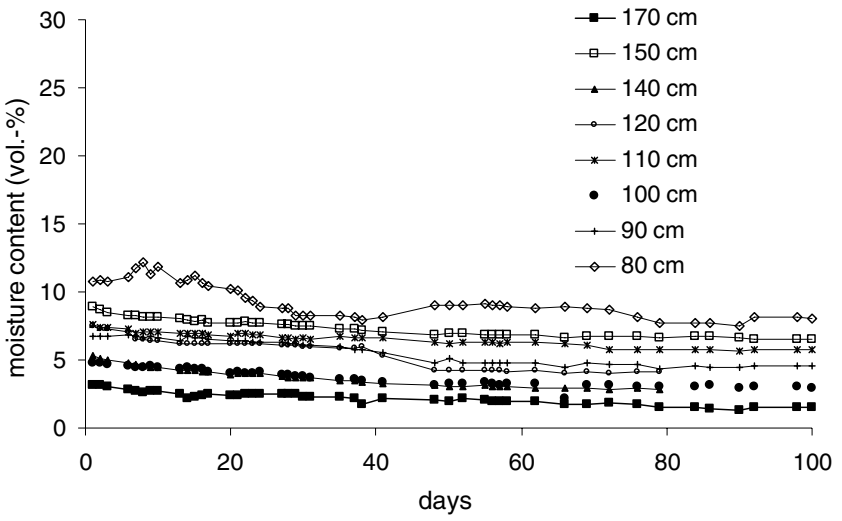

Fig. 5. Time series of measured moisture contents at different heights after discharging the column. Heights are given as distance to the bottom of the column.

4. Results and discussion

4.1. Sediment and initial pore water characteristics

The chemical characteristics of the material are compiled in Table 1. The sediment shows a low pyrite content and the small content of inorganic C indicates a low buffer capacity.

X-ray diffractometry analysis of sediment samples at the top of the column yielded traces of trivalent Fe-sulphate minerals such as jarosite which are reported to form below a pH of 2. Furthermore quartz, gypsum, mica, chlorite and traces of smectite were identified.

The entire sediment core of the observation borehole shown in Fig. 1 was analysed for pyrite contents and yielded a depyritisation depth of approximately 12 m which has resulted from pyrite weathering during the last 30 a (Fig. 6). Pyrite in the uppermost 12 m has been almost completely oxidized indicating a high reactivity.

Analyses of grain size of pyrite in the Lusatian mining district carried out by Berger (2000) yielded predominantly framboidal structures showing grain sizes between 0.1 and 30 μm. Owing to the generally large internal surface area of framboids, Berger (2000) supposed a high reactivity of pyrite. This is supported by the extremely low pyrite contents which were found in the uppermost 12 m of the sediment core and which are due to almost complete pyrite oxidation.

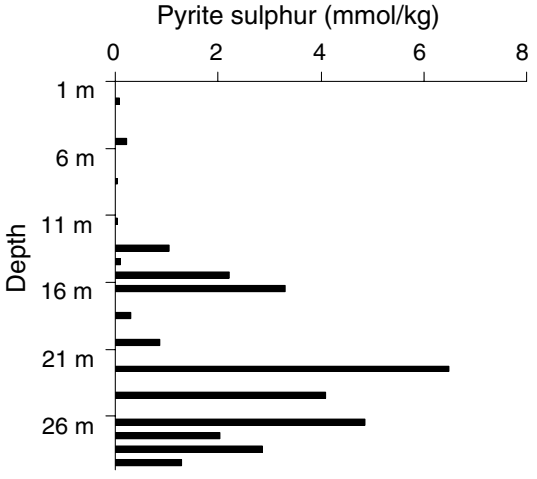

Fig. 6. Analysed pyrite sulphur of waste dump sediments at the well location (Fig. 1). The material of the column study core was taken from the same sediment core. The groundwater level is 12 m below surface.

The initial pore water composition analysed before draining the column indicated slightly acid conditions which were due to the originally anaerobic conditions and to the dilution of the original pore water with distilled anaerobic water (Table 3). The low alkalinity leads to the conclusion that buffering of pH by calcite dissolution is of minor importance. The molar ratios evidence that SO_4^{2-} has mainly originated from gypsum dissolution.

4.2. Column study

The measured breakthrough curves are shown in Fig. 7. The O_2 saturation increased from nearly 0% in all oxygen probes to full saturation in the upper probes and 20–30% in the lower parts of the column. The measured breakthrough curves at 175 and 155 cm height show an immediate sharp increase of O_2 saturation from the beginning of the experiment in the uppermost part of the column on the first day. This was due to the advective input of atmospheric gas originating from draining the column. The sharp decrease of O_2 concentrations within the next 2 days can only be explained by major consumption of O_2 due to pyrite oxidation. As soon as the diffusive delivery of O_2 exceeded O_2 consumption, O_2 concentrations started to increase.

The lower probes show an increasing delay of O_2 rise with depth due to the presence of pyrite, whose oxidation constitutes a sink term for O_2. As soon as the zone of depyritisation had migrating downwards, the O_2 saturation begins to increase owing to delivery of O_2 primarily by molecular diffusion.

4.3. Calibration procedure

In the first simulation using the input parameters defined in Table 2 the slopes of the calculated breakthrough curves are steeper than the measured results (Fig. 7). To fit the modelled results the initial tortuosity factor calculated by the original code of SAPY according to Eqs. (4) and (5) had to be adjusted, resulting in the following calibrated dependence of tortuosities on waterfilled porosity (Fig. 8):

$$\tau = 2.5 \times \ln(nw) + 12.488 \quad (16)$$

where nw stands for waterfilled porosity and τ represents tortuosity.

This calibrated logarithmic dependence of tortuosity on waterfilled porosity, which results in higher tortuosities was implemented in the original SAPY

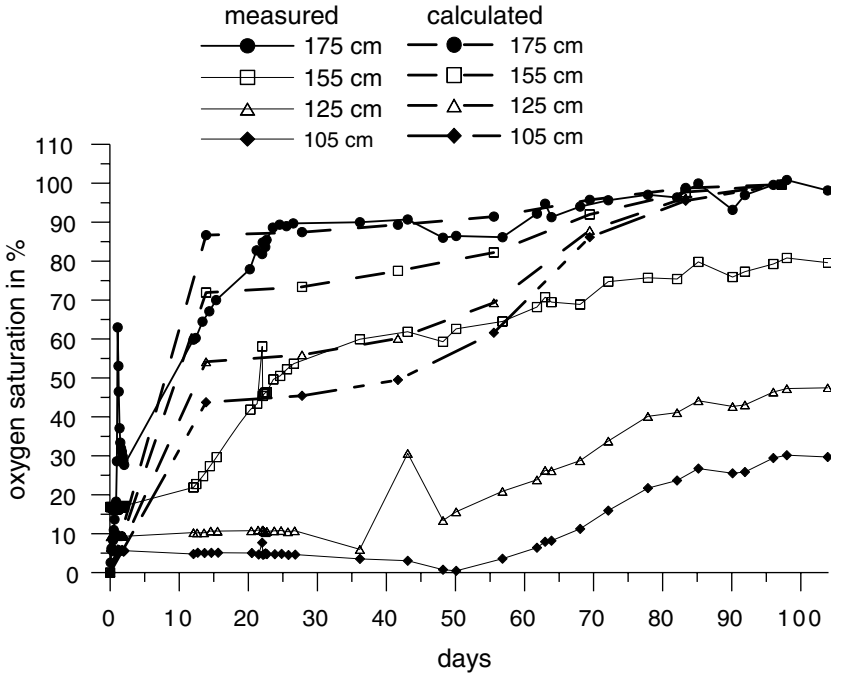

Fig. 7. Measured and calculated breakthrough curves of O_2 at different heights of the column before calibration.

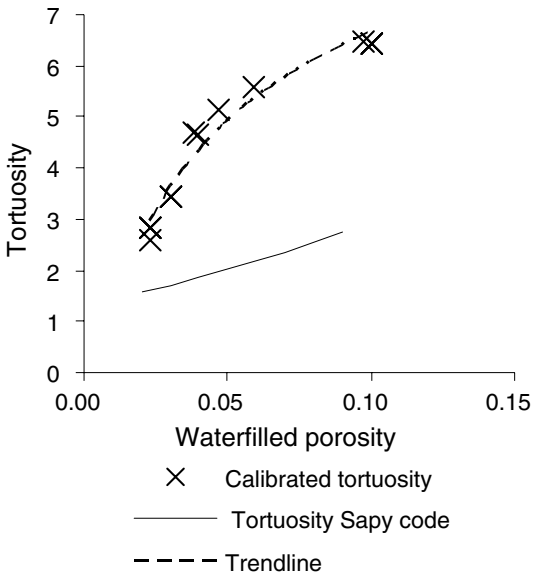

Fig. 8. Dependence of tortuosity on waterfilled porosity. The solid line represents the relationship initially implemented in the SAPY code. Cross symbols show the calibrated tortuosities for different moisture contents.

code and can be used for future calculations of this type of sediment within the range of 0.02–0.1 for the waterfilled porosity.

In principle, the mismatch of measured and calculated O_2 concentrations before calibration could also be due to underestimated microbial mediation factors, as microbial mediation is site specific. To verify this statement, simulations were performed with larger microbial mediation factors yielding identical calculated O_2 breakthrough curves. Reducing microbial mediation factors leads to even steeper calculated breakthrough curves resulting in a worse fit with the measured data. Therefore a better fit of calculated values could not be obtained by changing the biotic rate expressions originally implemented in SAPY. This leads to the conclusion that the diffusive O_2 delivery through the sediment is the limiting factor controlling the oxidation rate.

4.4. Model results

The final results of fitting the simulated curves to observed O_2 concentrations are shown in Fig. 9. Small jumps within the calculated curves of O_2 concentrations are due to the spatial discretisation of the numerical model. They occur when a cell becomes free of pyrite within the calculations and leads to an enhanced diffusive delivery of O_2. At all heights 3 different stages can be distinguished with regard to the simulated O_2 concentrations.

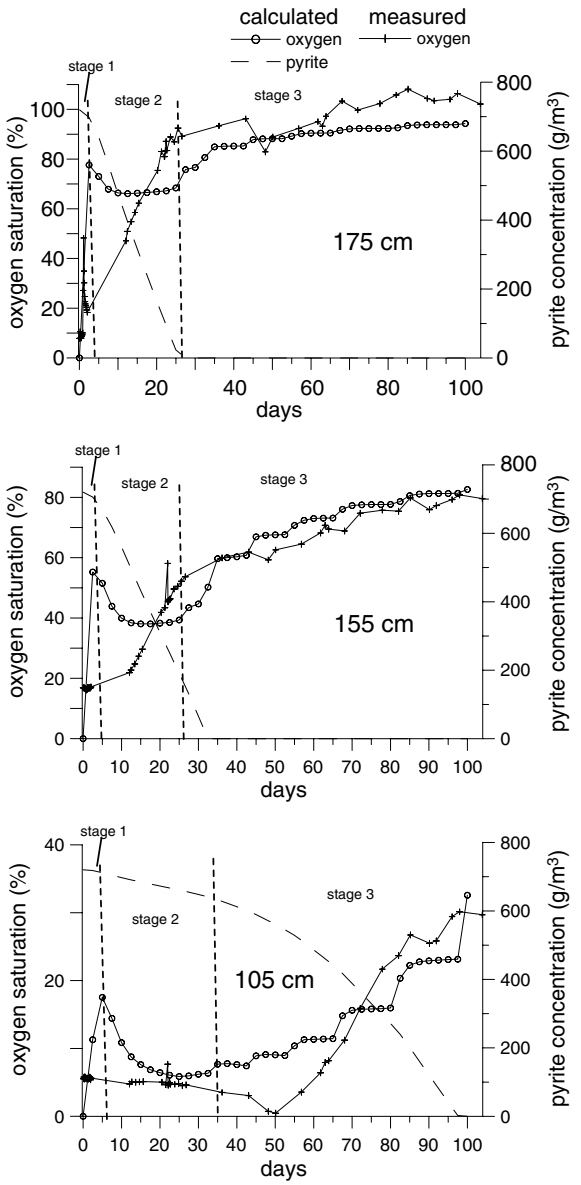

Fig. 9. Measured O_2 concentrations and calculated pyrite and O_2 concentrations after calibration at 105, 155 and 175 cm height of the column. Vertical dotted lines represent different stages.

The first stage reflects a sharp increase of simulated O_2 within the first 5 days of the experiment due to diffusive O_2 delivery without O_2 consumption. This results from the delayed microbial acceleration of pyrite oxidation in the model calculations, which does not start until the simulated pH has dropped to a value of 3. When the simulated pH is below 3, the oxidation rate of pyrite is accelerated up to 5 magnitudes as documented in Fig. 4. This leads to decreasing O_2 concentrations until the equilibrium between diffusive O_2 delivery and O_2 consumption is reached and is reflected in stage 2. Afterwards O_2 delivery exceeds consumption and the calculated O_2 concentrations start to rise (stage 3). Calculated pyrite contents in Fig. 9 indicate that calculated O_2 starts to increase sharply after the pyrite of the respective cells has been consumed.

The general trend of the measured data could be reproduced by the simulation. However, several discrepancies are obvious and are related mainly to the implementation of microbiological catalysis in SAPY. Owing to the few available data within the first 10 days a possible time delay of microbiologic activity (stage 1) cannot be proved by measured data so far in this study. An interesting point is the measured O_2 concentrations at 105 cm height, which do not increase until day 50 but which show a steep increase from day 50 onwards. This breakthrough curve indicates that consumption of O_2 had exceeded diffusive delivery of O_2 until day 50. Here the oxidation rates which are necessary to consume O_2 delivered by diffusion are much higher than abiotic oxidation rates for pyrite and indicate microbial acceleration. Comparison of this breakthrough curve with the simulated results suggests that microbial acceleration is underestimated in SAPY.

The calculated pyrite contents yield a depyritisation depth of ≈1 m after 100 days. Since the column was flooded after exposure to atmospheric O_2 no sediment samples could be taken after the draining period of the column experiment to verify the simulated data. For comparison, a column study of Hecht and Kölling (2002) yielded a depth of depyritisation of 0.6 m after 200 days with sediment containing 1.2 wt% of pyrite. Analysed data at the field site show a depyritisation depth of 12 m after 30 a of exposure to atmospheric O_2 (Fig. 6).

The experimental determination of the normal rate of diffusion without pyrite is problematic in these sediments because of the formation of secondary minerals, which are present after the oxidation of pyrite. These minerals lead to reduced pore volumes and elevated tortuosities which inhibit the direct experimental determination of the effect of pyrite oxidation on the diffusive delivery of O_2. Therefore no parallel column study with non-sulphidic sediments from the study area was carried out.

To gain some idea about the rate of diffusion in this sediment without pyrite and about the effect of microbial mediated weathering rates of pyrite a

sensitivity study was carried out (Fig. 10). In the first scenario the initial pyrite content was set at zero. The simulation calculates much steeper breakthrough curves than the measured values yielding full O_2 saturation at 1 m depth after 30 days. This leads to the conclusion that O_2 consumption has to occur in the sediment. In a second scenario microbial mediation of the abiotic weathering rates was not allowed assuming a pyrite content of 0.04 wt%. The result is shown in Fig. 10 for a height of 105 cm in the column and yields O_2 concentrations very similar to the values calculated without pyrite. This provides evidence of the low amount of O_2 which is consumed without microbial catalysis of pyrite weathering.

4.5. Comparing calibrated tortuosities with data found in other studies

Usually the complex geometries of soils and other similar materials make it necessary to use equations that empirically relate the variable D/D_0 to soil structure parameters. Troeh et al. (1982) compiled different empirical approaches to this topic. To compare the results with other studies the following widely used equation was applied:

$$D/D_0 = Kn_a^m \tag{17}$$

where D_0 represents the molecular coefficient of diffusion, D stands for the effective diffusion coefficient, n_a means airfilled porosity, K and m are determined by fitting curves to experimental data.

The formulae derived by Marshall (1959); Millington (1960) and Penman (1940) overestimate the effective diffusion coefficients and cannot be applied to the sediments of the study area (Fig. 11). This is probably due to the strong heterogeneity of the material, which shows a great variety of grain sizes causing high tortuosities. A good fit was obtained using the empirical formula (Eq. (17)) with the fitting parameter $m = 5.7$ and $K = 34$. The parameter m represents pockets or incomplete passages of pore space, when diffusion ceases.

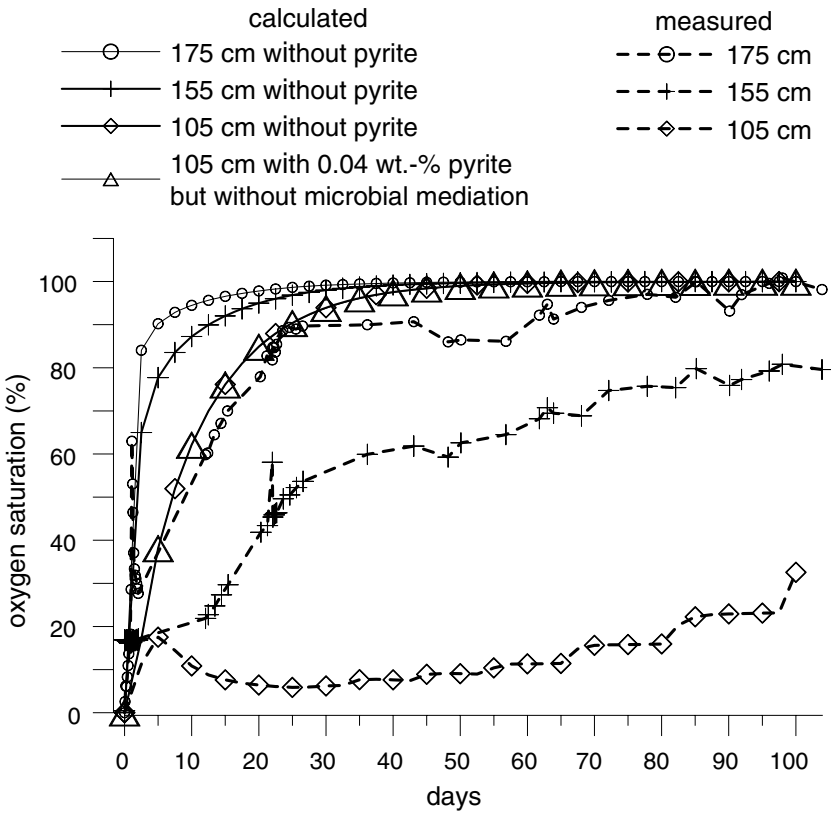

Fig. 10. Measured and calculated O_2 concentrations assuming (i) the absence of pyrite or (ii) the absence of microbial mediation. Dotted lines represent measured O_2 concentrations at different heights of the column, solid lines indicate calculated concentrations.

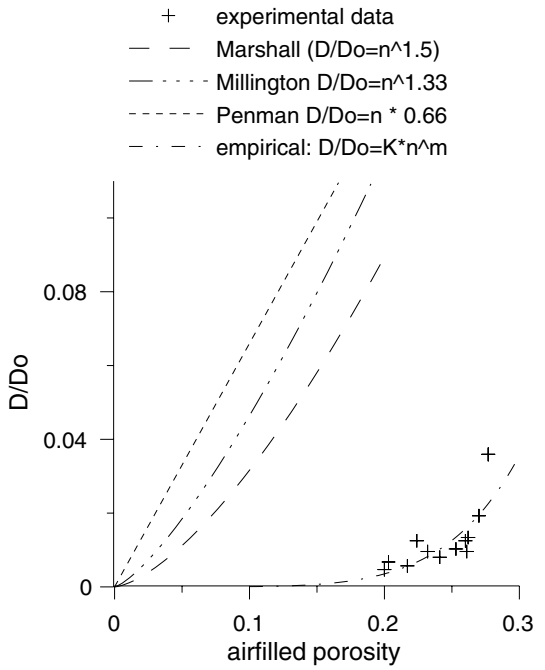

Fig. 11. Dependence of effective diffusion on airfilled porosity. D is the effective diffusion coefficient ($L^2\,t^{-1}$) and D_0 is the molecular diffusion coefficient of oxygen in nitrogen ($L^2\,t^{-1}$). Cross symbols represent the effective diffusion coefficients obtained from the column test, lines represent the relationship found in diffusion tests for different sediments found by other authors.

4.6. Model limitations

The presented modelling approach does not consider precipitation of minerals. This may lead to erroneous predictions for example for the release of SO_4^{2-} from a waste dump if the pore water is oversaturated in gypsum. However, this point is of minor importance in this study, since the column was not irrigated in the experiment. A further restriction is the strong dependency of both effective diffusion and microbial mediated oxidation rates on site-specific conditions. Therefore an application of this approach to another area can only be realized after a careful calibration and verification of the model using experimental data. A further point is the restriction to one-dimensional processes which makes it difficult to treat two- or three-dimensional field problems.

4.7. Upscaling and application

In spite of the number of limitations the column test and its modelling approach has a clear relevance for the remediation of environmental problems. Beside the interpretation of one-dimensional column tests, the application of this study consists in developing a method for predicting the release of SO_4^{2-} from waste dumps. The results of this research were scaled up to field conditions in a new model which was verified by observed O_2 and SO_4^{2-} data of the waste dump (Kohfahl and Pekdeger, 2004). To reproduce the observed data Eq. (16) had to be adapted by reducing the tortuosities for given moisture contents. This leads to the conclusion that the undisturbed natural sediment shows higher permeabilities and there are a couple of possible reasons for the discrepancy between field and laboratory data. One reason might be that the calibrated dependence of tortuosity on the moisture content of the sediment was derived for sediments with a waterfilled porosity smaller than 0.1 and cannot be extrapolated to waterfilled porosities greater than 0.2 which were measured in the field. Another possible explanation is the existence of preferential pathways for gas through sedimentary structures in the field, which do not exist in the column. A further reason might be the local variability of the sediment material in the heap, which shows a higher proportion of coarse grained material at the observation well of the field measurements in comparison to the sediment material used in the column.

For prognostic purposes different scenarios of field conditions were simulated for the next 80 a in order to gain some idea about the future the mass input of SO_4^{2-} into the groundwater and the surrounding surface water (Kohfahl and Pekdeger, 2004).

5. Conclusions

This paper presents the results of detailed O_2 measurements in a column filled with pyrite bearing sediments during a diffusion experiment and a modelling approach which allowed the successful simulation of this experiment. The study showed that O_2 delivery in the gas phase led to the full depletion of pyrite within the first meter of sediment from the top of the column during a period of 100 days. From the model calibration a new empirical formulation was derived describing the dependence of tortuosity on moisture content. The simulations clearly indicate that oxidation rates of pyrite were elevated, most likely due to microbial catalysis. Further, it could be shown that the rate of diffusive O_2 delivery is generally below the biotic oxidation rate and thus

a limiting factor for pyrite oxidation under unsaturated conditions. After upscaling, the model could be successfully applied to field conditions in the study of Kohfahl and Pekdeger (2004), in which its usefulness and robustness for management and predictive issues was well demonstrated.

Acknowledgements

We particularly thank Henrik Hecht and Martin Kölling for their contributions and support concerning fiber optic oxygen measurements. This study was financed by BMBF and LMBV.

References

Ahonen, L., Tuovinen, O.H., 1989. Microbiological oxidation of ferrous iron at low temperatures. Appl. Environ. Microbiol. 2, 312–316.

Albertsen, M., 1977. Labor- und Felduntersuchungen zum Gasaustausch zwischen Grundwasser und Atmosphäre über natürlichen und verunreinigten Gewässern. PhD thesis Thesis, Christian-Albrechts-Univ. zu Kiel, Kiel.

Berger, W., 2000. Stoffinventar und Stoffänderungen durch Redoxreaktionen in Sedimenten des Lausitzer Braunkohlereviers. Proceedings des Dresdner Grundwasserforschungszentrum e.V, 18. Selbstverlag des Herausgebers, Dresden.

Chavaire, C., Karamanev, D., Godard, F., Garnier, A., Andre, G., 1993. Comparison of the kinetics of ferrous iron oxidation by three different strains of *Thiobacillus ferrooxidans*. Geomicrobiol. J. 11, 57–63.

Cornish Bowden, A., 2004. Fundamentals of Enzyme Kinetics. Portland Press, London.

Crank, J., 1956. The Mathematics of Diffusion. Oxford University Press, London.

Currie, J.A., 1970. Movement of gases in soil respiration. In: Soils Soc. Chem. Ind. (Ed.), Sorption and Transport Processes in Soils. London, pp. 152–171.

Curutchet, G., 1992. Effect of iron (III) and its hydrolosis products of *Thiobacillus ferrooxidans*. Biotechnol. Lett. 14, 329–334.

Davis, G.B., Ritchie, A.I.M., 1986. A model of oxidation in pyritic mine waste. Part I: equations and approximate solutions. Appl. Math. Model. 10, 314–322.

Davis, G.B., Ritchie, A.I.M., 1987. A model of oxidation in pyritic mine waste. Part III: importance of particle size distribution. Appl. Math. Model. 11, 417–422.

Davis, G.B., Doherty, G., Ritchie, A.I.M., 1986. A model of oxidation in pyritic mine waste. Part II: comparison of numerical and approximate solution. Appl. Math. Model. 10, 323–329.

Eberling, B., Nicholson, R.V., 1996. Field determination of sulphide oxidation rates in mine tailings. Water Resour. Res. 32, 1773–1784.

Eberling, B., Larsen, F., Christensen, S., Postma, D., 1998. Gas transport in a confined unsaturated zone during atmospheric pressure cycles. Water Resour. Res. 34, 2855–2862.

Falta, R.W., Javandel, I., Pruess, K., Witherspoon, P.A., 1989. Density driven flow of gas in the unsaturated zone due to the evaporation of volatile organic compounds. Water Resour. Res. 25, 2159–2169.

Foos, A., 1997. Geochemical modelling of coal mine drainage, Summit County, Ohio. Environ. Geol. 31, 205–210.

García, C., Ballester, A., González, F., Blazquez, F.L., 2005. Factors affecting the transformation of a pyritic tailing: scaled-up column tests. J. Hazard. Mater. 118, 35–43.

Hecht, H., Kölling, M., 2001. A low-cost optode array measuring system based on 1 mm plastic optical fibers – new technique for in situ detection and quantification of pyrite weathering processes. Sensors Actuat. B 81, 76–82.

Hecht, H., Kölling, M., 2002. Investigation of pyrite-weathering processes in the vadose zone using optical oxygen sensors. Environ. Geol. 42, 800–809.

Hecht, H., Kölling, M., Geissler, N., 2003. DiffMod7 – Modeling Oxygen Diffusion and Pyrite Decomposition in the Unsaturated Zone Based on Ground Air Oxygen DistributionGeochemical Processes – Concepts for Modeling Reactive Transport in Soils and Groundwater. Wiley-VCH, Weinheim, pp. 55–76.

Hendershot, W.H., Duquette, M., 1986. A simple barium chloride method for determining cation exchange capacity and exchangeable cations. Soil Sci. Soc. Am. J. 50, 605–608.

Hsieh, Y.P., Yang, C.H., 1989. Diffusion methods for the determination of reduced inorganic sulfur species in sediments. Limnol. Oceanog. 34, 1126–1130.

Karavaiko, G.I., Kovalenko, T.V., Piskunov, V.P., 1982. Effect of Fe(III)-ions in the oxidation of ferrous iron by *Thiobacillus ferrooxidans* at various temperatures. Microbiologyia 51, 156–160.

Kargbo, D.M., He, J., 2004. A simple accelerated rock weathering method to predict acid generation kinetics. J. Environ. Geol. 46, 775–783.

Kirby, C.S., Elder Brady, J.A., 1998. Field determination of Fe^{2+} oxidation rates in acid mine drainage using a continuously-stirred tank reactor. Appl. Geochem. 13, 509–520.

Kohfahl, C., Pekdeger, A., 2004. Modelling the long-term release of sulphate from dump sediments of an abandoned open pit lignite mine. Mine Water Environ. 23, 12–19.

Kohfahl, C., Pekdeger, A., 2006. Rising groundwater tables in partly oxidized pyrite bearing dump-sediments: Column study and modelling approach. J. Hydrol. 331, 703–718.

Kölling, M., 1990. Modellierung geochemischer Prozesse im Sickerwasser und im Grundwasser. no. 8, Fachbereich Geowissenschaften der Universität Bremen, Bremen.

Lacey, D.T., Lawson, F., 1970. Kinetics of the liquid-phase oxidation of acid ferrous sulfate by the bacterium *Thiobacillus ferrooxidans*. Biotechnol. Bioeng. 12, 29–50.

Landolt-Börnstein, 1969. Zahlenwerte und Funktionen aus Naturwissenschaft und Technik. Transportphänomene I: Diffusion in Gasen, Diffusion in Flüssigkeiten. 6. Auflage, Gruppe II, Band 5a. Springer-Verlag, Berlin, Heidelberg, New York.

Lowson, R.T., 1982. Aqueous oxidation of pyrite by molecular oxygen. Chem. Rev. 82, 461–497.

Marshall, T.J., 1959. The diffusion of gases through porous media. J. Soil Sci. 10, 79–82.

Mayer, K.U., 2002. Multicomponent reactive transport modeling in variably saturated porous media using a generalized formulation for kinetically controlled reactions. Water Resour. Res. 38, 1174–1195.

Millington, R.J., 1960. Transport in porous media. Trans. 7th Internat. Congr. Soil Sci., 97–106.

Nemati, M., Webb, C., 1997. A kinetic model for biological oxidation of ferrous iron by *Thiobacillus ferrooxidans*. Biotechnol. Bioeng. 53, 478–486.

Noike, T., Nakamura, K., Matsumoto, J., 1983. Oxidation of ferrous iron by acidophilic iron-oxidizing bacteria from a stream receiving acid mine drainage. Water Res. 17, 21–27.

Nordstrom, D.K., 1982. Aqueous pyrite oxidation and the consequent formation of secondary iron minerals. In: Nordstrom, D.K. (Ed.), Acid Sulphate Weathering. Soil Sci. Soc. Am., Spec. Publ. No. 10, pp. 37–56.

Nordstrom, D.K., 1985. The rate of ferrous iron oxidation in a stream receiving acid mine effluent. In: U.S.G.S. (Ed.), Selected Papers in the Hydrologic Sciences. Water Supply Paper 2270, Washington, DC, pp. 113–119.

Nyavor, K., Egibor, N.O., Fedorak, P.M., 1996. The effect of ferric ion on the rate of ferrous oxidation by *Thiobacillus ferrooxidans*. Appl. Microbiol. Biotechnol. 4, 688–691.

Okereke, A., Stevens, S.E., 1991. Kinetics of iron oxidation by *Thiobacillus ferrooxidans*. Appl. Environ. Microbiol. 57, 1052–1056.

Pantelis, G., Ritchie, A.I.M., 1991. Macroscopic transport mechanisms as rate limiting factor in dump leaching of pyritic ores. Appl Math. Model. 15, 136–143.

Penman, H.L., 1940. The diffusion of vapours through porous solids. J. Agric. Sci. 30, 437–463.

Pesic, B., Oliver, D.J., 1989. An electrochemical method of measuring the oxidation rate of ferrous to ferric iron with oxygen in the presence of *Thiobacillus ferrooxidans*. Biotechnol. Bioeng. 33, 428–439.

Prein, A., 1993. Sauerstoffzufuhr als limitierender Faktor für die Pyritverwitterung in Abraumkippen, Mitt. des Inst. Wasserwirtsch., Hydrologie und landwirtsch. Wasserbau Univ. Hannover. Inst. Wasserwirtsch., Hydrologie und landwirtsch.

Prein, A., Mull, R., 1998. Oxygen as a limiting factor for pyrite weathering in the overburden of open pit lignite areas. In: Geller, W., Klapper, H., Salomons, W. (Eds.), Acidic Mine Lakes. Springer, Berlin, pp. 237–250.

Scanlon, B.R., Nicot, J.P., Massmann, J.W., 2002. Soil gas movement in unsaturated systems. In: Warwick, A.W. (Ed.), Soil Physics Companion. CRC Press, pp. 297–341.

Schnaitman, C.A., Korczynski, M.S., Lundgren, D.C., 1969. Kinetic studies of iron oxidation by whole cells of *Ferrobacillus ferrooxidans*. J. Bacteriol. 99, 552–557.

Schwan, M., Fischer, R., Dybek, K., 1988. Prognose von Acidität, Eisen- und Sulfatkonzentration im Grundwasser von Bergbaugebieten. Acta Hydrochim. Hydrobiol. 16, 579–588.

Simunek, J., Suarez, D.L., 1993. Modeling of carbon-dioxide transport and production in soil. 1. Model development. Water Resour. Res. 29, 487–497.

Singer, P.C., Stumm, W., 1970. Acidic mine drainage: the rate determining step. Science 167, 1121–1123.

Strömberg, B., Banwart, S., 1994. Kinetic modeling of geochemical processes at the Aitik mining waste rock site in northern Sweden. Appl. Geochem. 9, 583–595.

Stumm, W., Lee, G.F., 1961. Oxygenation of ferrous iron. Ind. Eng. Chem. 53, 143–146.

Troeh, F.R., Jalal, D.J., Kirkham, D., 1982. Gaseous diffusion equations for porous materials. Geoderma 27, 239–253.

Walter, A.L., Frind, E.O., Blowes, D.W., Ptacek, C.J., Molson, J.W., 1994a. Modeling of multicomponent reactive transport in groundwater. Model development and evaluation. Water Resour. Res. 30, 3137–3148.

Walter, A.L., Frind, E.O., Blowes, D.W., Ptacek, C.J., Molson, J.W., 1994b. Modeling of multicomponent reactive transport in groundwater, Metal mobility in aquifers impacted by acidic mine tailings discharge. Water Resour. Res. 30, 3149–3158.

Weber, P.A., Stewart, W.A., Skinner, W.M., Weisener, C.G., Thomas, J.E., Smart, R.St.C., 2004. Geochemical effects of oxidation products and framboidal pyrite oxidation in acid mine drainage prediction techniques. Appl. Geochem. 19, 1953–1974.

Williamson, M.A., Rimstidt, J.D., 1994. The kinetics and electrochemical rate determining step of aqueous pyrite oxidation. Geochim. Cosmochim. Acta 58, 5443–5454.

Wunderly, M.D., Blowes, D.W., Frind, E.O., Ptacek, C.J., 1996. Sulfide mineral oxidation and subsequent reactive transport of oxidation products in mine tailings impoundments - a numeric model. Water Resour. Res. 32, 3173–3187.

Xu, T., White, S.P., Pruess, K., Brimhall, G.H., 2000. Modeling of pyrite oxidation in saturated and unsaturated subsurface flow systems. Trans. Porous Media 39, 25–56.